Remote Blood Pressure Estimation from Facial Videos using Transfer Learning: Leveraging PPG to rPPG Conversion

Chun-Hong Cheng[1*] Jing Wei Chin[1,2] Kwan Long Wong[1,2] Tsz Tai Chan[1,2]
Hau Ching Lo[2] Kwan Lok Pang[2] Richard So[2†] Bryan Yan[3]
[1]PanopticAI [2]Hong Kong University of Science and Technology [3]Chinese University of Hong Kong

Abstract

Blood pressure (BP) monitoring is crucial for health assessment, but existing contact-based methods face cost and comfort barriers. Remote photoplethysmography (rPPG) offers a promising contactless solution, yet research is hampered by limited rPPG datasets with corresponding BP labels. This paper presents a transfer learning methodology for BP measurement. This approach involves utilizing a base dataset comprising signals produced by PPG (PPG-signals) to acquire knowledge that can be transferred to a target dataset containing signals generated by rPPG (rPPG-signals). In our study, we trained diverse deep-learning models using publicly available datasets containing PPG-signals. Subsequently, these models were fine-tuned and evaluated using a public dataset that specifically consists of rPPG-signals. Additionally, we explored the relationship between BP and heart rate, and examined different loss functions and normalization approaches to optimize the performance of the deep learning models. The findings of our study demonstrate that our best model achieved a better performance than the state-of-the-art model, with mean absolute error (MAE) of 8.721 (reduced by 4.879) mmHg and 8.653 (reduced by 1.647) mmHg for systolic blood pressure (SBP) and diastolic blood pressure (DBP) in a dataset with clinical settings, showing promising potential for remote BP estimation.

1. Introduction

Blood pressure (BP) is a crucial physiological factor for identifying any potential cardiovascular disease of a subject [24, 74]. Cuff-based methods based on oscillometry [48, 65, 67, 78] and sphygmomanometers [5, 35, 40, 72] have been generally used for measuring BP over the past decades. However, they are not suitable for long-term monitoring as they may cause discomfort and irritation to people with sensitive skin.

To overcome these limitations, cuffless methods have been developed for continuous BP monitoring, especially utilizing signals produced by photoplethysmography (PPG-signals) and machine learning methods [2, 16, 21–23, 27, 46, 68, 69, 71, 75, 83]. PPG-signals are frequently used to assess other vital signs as well, including heart rate (HR) [6,58,61], respiratory rate [9,47,53] and blood oxygen saturation (SpO_2) [3,8,59]. They involve employing a light emitter and sensor to gauge the fluctuations in blood vessel volume beneath the skin. When tissue is exposed to light, the photodetector records slight changes in light intensity caused by blood flow [51]. However, they are still contact-based approaches and cannot provide a pain-free solution. Therefore, using signals generated by remote photoplethysmography (rPPG-signals) have emerged as a promising approach for remote vital sign monitoring.

In the last decade, significant strides have been made in developing sophisticated algorithms for the extraction of rPPG-signals from human skin [18, 45, 62, 63, 76]. These methods typically entail the utilization of digital imaging devices such as webcams or regular RGB cameras, which function as sensors to detect minute alterations in skin color, with natural light in the environment serving as the illumination source [13]. Following the extraction of rPPG-signals, subsequent stages involve signal filtering techniques, and frequency domain analyses are performed to estimate desired vital signs. With advancements in computer science and artificial intelligence, deep learning algorithms have emerged as front-runners, achieving state-of-the-art performance in remote vital sign monitoring, especially for HR [26, 31, 44, 82] and SpO_2 [33, 52, 60, 70]. However, for BP, estimation performance remains suboptimal, necessitating further refinement before practical deployment in real-world scenarios [17, 20, 50].

Machine learning methods that use either PPG-signals or rPPG-signals for BP prediction are generally based on two categories: feature extraction and deep learning-based end-to-end prediction. The former extracts and utilizes handcrafted features in the time and frequency domain to train

*Corresponding author (email: keithcheng@panoptic.ai)
†Supervisor

models for BP prediction. The latter derives features from PPG-signals or rPPG-signals directly with deep learning models, and these models learn how to predict BP from such implicitly extracted features. To achieve state-of-the-art performance when using deep learning methods, especially in supervised learning, a considerable amount of data is usually required. However, to the best of our knowledge, there are only a few public datasets [66, 84] that contain extracted rPPG-signals or facial videos with BP information that could be used as a reference for training deep learning models.

In this paper, to address the data scarcity issue, we adopt a transfer learning approach to estimate BP with the use of PPG-signals and rPPG-signals. Deep learning models are first trained with PPG-signals and HR to predict systolic blood pressure (SBP) and diastolic blood pressure (DBP), as HR has been observed to correlate with BP [42] with the assumption of the absence of HR hysteresis. These pre-trained models are then fine-tuned with rPPG-signals and HR. All datasets used are publicly available, allowing for fair comparison of different proposed methods. Furthermore, different loss functions and normalization approaches are explored to optimize the performance of the models.

2. Literature Review

2.1. PPG-based Blood Pressure Estimation with Machine Learning

Slapničar et al. [68] utilized handcrafted features extracted from filtered PPG-signals to train multiple regression models. These models formed an ensemble of regressors to predict BP. In their later work, they introduced modifications to the ResNet architecture [30] by incorporating spectro-temporal blocks for BP estimation in an end-to-end manner using PPG-signals and their derivatives.

Hajj and Kyriacou [21] initially extracted features from filtered PPG-signals and fed selected effective features to gated recurrent units (GRU) [15] to estimate BP. In their subsequent work [22], they enhanced their approach by incorporating features derived from the first and second derivative of PPG-signals, and applied an attention mechanism for effective feature extraction.

Esmaelpoor et al. [23] designed a multistage model integrating 1D convolutional neural network (CNN) and Long Short-Term Memory (LSTM) [32] to extract both short-term and long-term temporal features of PPG-signals for BP prediction.

Liang et al. [46] utilized a U-Net-based model [64] to reconstruct arterial blood pressure (ABP) signals from PPG-signals, subsequently determining SBP and DBP as the maximum and minimum values, respectively, of the reconstructed ABP signal.

Wang et al. [75] introduced an end-to-end BP estimation deep learning model featuring improved multi-scale fusion blocks to extract both local and global features from PPG-signals effectively.

2.2. rPPG-based Blood Pressure Estimation with Machine Learning

Wu et al. [81] employed the POS algorithm [76] to extract rPPG-signals from multiple regions of interest (ROIs) on the face, which were then passed into a 2D CNN for feature extraction. These features, along with others extracted from physiological indicators, were used to estimate BP.

To address data scarcity in rPPG-signals, Wu at al. [80] leveraged InfoGAN [11] to generate synthetic rPPG-signals. Additionally, they incorporated personal information such as body mass index (BMI) and age to enhance the realism of the generated rPPG-signals for BP prediction.

Iuchi et al. [34] split faces into multiple ROIs and extracted rPPG-signals with the method proposed in [25] for each ROI. These signals were then reconstructed into 2D inputs for retaining the spatial relationship of rPPG-signals, and fed into a 2D CNN to estimate BP.

Chen et al. [12] utilized 2D spatiotemporal feature map slices (STSs) to capture both spatial and temporal features from facial videos. This approach was also commonly used to predict other vital signs such as HR [49, 54–57] and SpO_2 [1, 14]. These STSs were then directly fed into a model, which comprised a combination of a deep residual network and LSTM to estimate BP.

Han et al. [29] focused on utilizing features extracted from rPPG-signals (green channel on the face) based on cardiovascular knowledge. These extracted features are potentially related to four factors, namely HR, stroke volume, peripheral vascular resistance and vessel wall elasticity. These features were then fed into a Bayesian neural network (BNN) for BP estimation.

Han et al. [28] stressed the importance of retaining shape details in pulse signals for BP prediction. They proposed an approach to transform rPPG-signals generated from a transformer model into average cardiac cycle (ACC) signals to minimize shape errors. Pulse-related features extracted from ACC signals were then utilized for BP prediction.

Chen et al. [10] applied Euler video magnification (EVM) to facial and hand videos in order to capture tiny skin color changes effectively. rPPG-signals (green channel) were then extracted from these enhanced videos, followed by signal filtering and feature extraction based on PTT. Multiple base regressors were trained and the estimation from each base regressor was further utilized to train a meta regressor to estimate BP.

Only one study [12] mentioned previously tried to estimate BP directly from facial videos, skipping the step of extracting rPPG-signals. This may be due to the explainability of the proposed solution. There are significantly more stud-

ies focused on discussing the relationship between BP and PPG-signals, and the performance of rPPG-signal extraction algorithms from facial videos. The black box nature of predicting BP directly from facial videos hinders the potential for being applied in the medical domain.

Moreover, most of the existing methodologies were evaluated using self-collected datasets, which greatly limits the comparability of algorithms. In addition, some reported results might be susceptible to data leakage, as data splitting was performed solely based on the number of samples instead of subjects, possibly leading to subject overlapping between training and test sets.

2.3. Transfer Learning with PPG-signals and rPPG-signals

Transfer learning is a technique commonly used in deep learning for efficient knowledge acquisition in scenarios with limited data in the target domain. Since PPG-signals and rPPG-signals are extracted under similar principles, the knowledge learnt from using PPG-signals for BP prediction can aid in rPPG-based BP estimation.

Schrumpf et al. [66] explored the applicability of transfer learning methodologies, leveraging insights gained from PPG-based BP prediction, and applied them to the estimation of BP using rPPG-signals. Their attention was directed towards examining the effect of the length of the input PPG-signal and derivatives of PPG-signals on model performance.

Kim et al. [38] designed a U-Net-based model, and applied transfer learning with PPG-signals and rPPG-signals for BP prediction on the same clinical dataset used in [66]. However, they merely split samples based on a specific ratio for training and evaluation. This was problematic because one subject might have more than one rPPG data, and the splitting by ratio allowed data from the same subject being used in both training and evaluation. Consequently, we considered the model from Schrumpf et al. [66] as the state-of-the-art model in our study.

3. Materials and Methods

3.1. Deep Learning Models

In addition to the four deep learning models used in [66] for BP prediction with transfer learning — Alexnet [41], ResNet [30], BiLSTM and the model designed by Slapničar et al. [69], we also included a unidirectional LSTM (UniLSTM) and BP-Net [73] for benchmarking. We compared the performance of UniLSTM and BiLSTM to determine whether incorporating backward information flow in PPG-signals can enhance BP prediction accuracy. Furthermore, we investigated whether a U-Net-based model such as BP-Net, which reconstructs ABP signals, is more suitable for BP prediction. Moreover, most existing works for BP prediction were formulated as a multi-task learning problem, estimating both SBP and DBP using a single model. We also examined the performance of predicting SBP and DBP separately with two identical models. To ensure a fair comparison between UniLSTM and BiLSTM, their neural network architecture were designed to be identical, except for the direction of the LSTM layers. For BP-Net, we modified the original U-Net-based model by adding dense layers after the decoder part to predict SBP and DBP. Additionally, since HR is used as a feature for BP prediction, we concatenated it to the output tensor of the last flatten layer of Alexnet, ResNet and Slapničar et al., the last unidirectional LSTM layer of UniLSTM, the last bidirectional LSTM layer of BiLSTM, and the last decoder layer of BP-Net. For each model, all layers before the concatenated layer were frozen during fine-tuning, except for BP-Net, where only the encoder part was frozen.

3.2. PPG Datasets

3.2.1 MIMIC-III Subset from Kaggle

We utilized a subset of MIMIC-III that was released on Kaggle [1]. This dataset underwent preprocessing and cleaning steps outlined in [36] to ensure data validity. The ABP signals, electrocardiogram (ECG) signals and PPG-signals have a sampling rate of 125Hz, comprising a total of 12000 records collected over different periods. There may have been more than one record from one patient; however, determining that was not feasible.

3.2.2 MIMIC-III Subset from PulseDB

PulseDB [2] [77] is a huge dataset consisting of cleaned and validated data from MIMIC-III and VitalDB [43]. Various preprocessing techniques were applied to ensure data quality. Since the ABP signals and PPG-signals in VitalDB have a sampling rate of 500Hz, they were downsampled to 125Hz so that all data in PulseDB had the same sampling rate. Moreover, each record was segmented into non-overlapping 10-seconds signals, resulting in a total of 5,245,454 10-seconds signals. For our experiments, we ignored the data from VitalDB to avoid utilizing downsampled data.

3.3. rPPG Dataset from Leipzig University Hospital (rPPG-LUH)

rPPG-LUH was collected based on the work by Schrumpf et al. [66]. During data collection, an industrial USB camera operating at 32 frames per second (fps) was utilized to capture the face and upper body of patients in ICU for around 2 hours. After excluding subjects with poor

[1] MIMIC-III Subset. https://www.kaggle.com/datasets/mkachuee/BloodPressureDataset/data

[2] PulseDB Dataset. https://github.com/pulselabteam/PulseDB

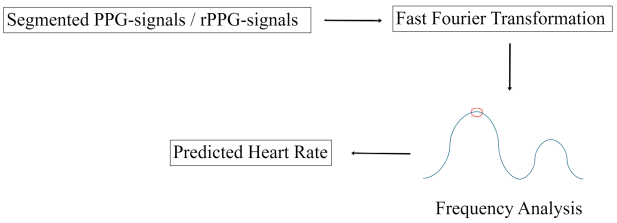

Figure 1. Process of estimating HR from PPG-signals / rPPG-signals.

illumination and motion artifacts, data of 17 subjects were publicly released for research purposes [3].

3.4. Data Preprocessing

3.4.1 PPG Data

Both PPG datasets were already preprocessed with multiple signal filtering methods upon access. We divided all PPG-signals in a non-overlapping manner with a window size of 7-seconds to match the length of the rPPG-signals. Because reference HR values were not provided, we estimated HR from each PPG-signal by applying Fast Fourier Transformation. HR was determined as the highest peak in the frequency domain that was within the normal HR range of 30 to 240 beats per minute [7, 19]. Figure 1 illustrates the procedure of determining HR from PPG-signals.

3.4.2 rPPG Data

In rPPG-LUH, rPPG-signals were first extracted using the POS algorithm. They were subsequently segmented with a window size of 7-seconds and then upsampled to 125 Hz by the authors to match the input length of their pretrained deep learning models [66]. To enhance BP prediction accuracy, we applied several noise removal procedures on these rPPG-signals. Initially, a Butterworth filter (4th order, 0.5Hz-8.0Hz cutoff frequency) was employed for signal filtering. Next, to remove low frequency noise that might result in baseline wander, wavelet transformation with db8 wavelet was applied. Finally, only signals with signal-to-noise ratio above -7 dB were retained. HR values were estimated using the same method depicted in Figure 1. Figure 2 also shows the preprocessed PPG-signals and rPPG-signals with respect to high and normal BP in different datasets.

3.5. Training Settings

3.5.1 Pretraining with PPG Data

For the MIMIC-III subset from Kaggle, the dataset was already divided into a training set with 9600 records and a

[3] rPPG-LUH. https://github.com/Fabian-Sc85/non-invasive-bp-estimation-using-deep-learning

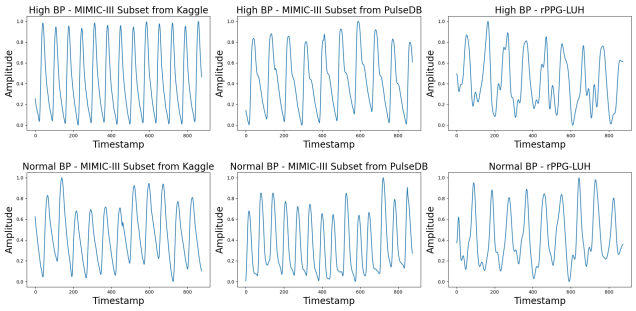

Figure 2. Visualisation of preprocessed PPG-signals and rPPG-signals with respect to high and normal BP in different datasets.

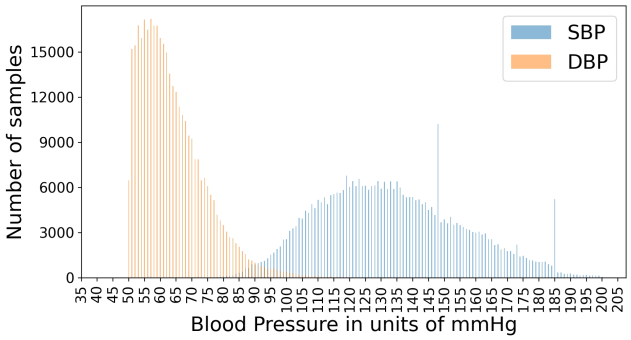

Figure 3. SBP and DBP distribution for the MIMIC-III subset from Kaggle.

test set with 2400 records by the authors [36]. For each segmented sample, the maximum and minimum values in the corresponding ABP signal were determined as SBP and DBP. Figure 3 shows the distribution of SBP and DBP for this dataset. For the MIMIC-III subset from PulseDB, the authors had already partitioned it into a training set, a calibration-free test set and a calibration-based test set [77]. Only the calibration-free test set, which did not share subjects with the training set, was used for evaluation. Figure 4 illustrates the distribution of SBP and DBP for this dataset. For these two datasets, two min-max normalization approaches were applied to explore optimized training settings for the deep learning models. The first one was applying min-max normalization on each individual PPG-signal in the training and test sets (per signal). The second one was first finding the maximum and minimum values among all PPG-signals in the training set and then applying min-max normalization on both training and test sets with those maximum and minimum values (per dataset). Each model was trained for 100 epochs with a batch size of 128. Adam optimizer [39] with learning rate = 0.001 was applied and mean squared error loss function was used to calculate the difference between predicted and reference labels (SBP and DBP), respectively.

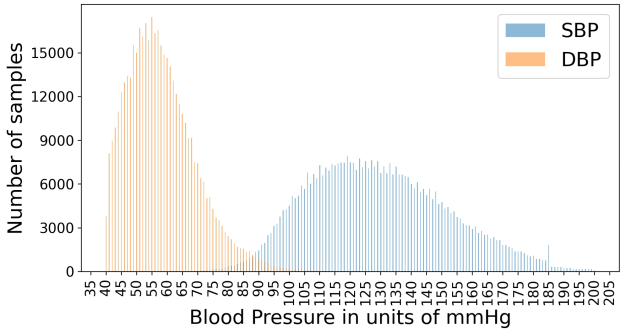

Figure 4. SBP and DBP distribution for the MIMIC-III subset from PulseDB.

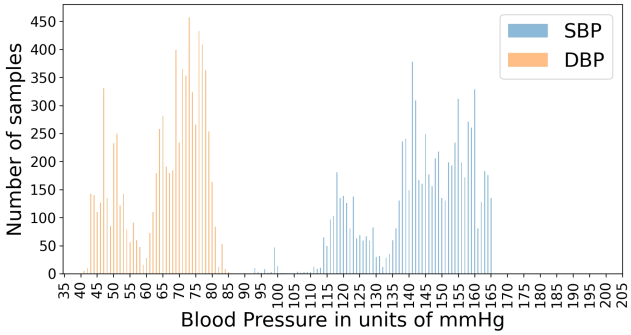

Figure 5. SBP and DBP distribution for the rPPG-LUH after preprocessing.

3.5.2 Transfer Learning with rPPG Data

Figure 5 presents the distribution of SBP and DBP for the rPPG-LUH. Notably, this dataset exhibits an imbalance, with a majority of the samples having SBP $>$ 130 (prehypertension) and DBP $>$ 60. Given the relatively limited number of samples in this dataset, 4-fold cross validation based on subjects was employed on the entire dataset, with 4-fold averaged results reported. This ensured that the training and test sets did not share any subject during training and evaluation. Two min-max normalization approaches were also utilized. The first one was applying min-max normalization on each individual rPPG-signal in the training and test sets (per signal). The second one was applying min-max normalization on both training and test sets with the maximum and minimum values determined in the pretrain stage (per dataset). Each model was trained for 100 epochs with a batch size of 32 and Adam optimizer (learning rate = 0.001). Mean absolute error (MAE) and mean squared error (MSE) loss functions were explored for performance comparison.

3.5.3 Performance Metrics

We used the mean absolute error (MAE) to monitor the performance of BP prediction during training and evaluation:

$$MAE = \frac{\sum_{i=1}^{N} |xsbp_i - ysbp_i|}{N} + \frac{\sum_{i=1}^{N} |xdbp_i - ydbp_i|}{N} \quad (1)$$

where $xsbp_i$ and $xdbp_i$ are the predicted SBP and DBP, respectively, and $ysbp_i$ and $ydbp_i$ are the reference SBP and DBP, respectively, in the unit of mmHg. For the case of single-task learning, only the single corresponding term in the expression is used.

4. Results and Discussion

4.1. Blood Pressure Estimation with PPG Data

Figures 6 and 7 present the performance of the models averaged by all training settings for SBP and DBP prediction on different PPG datasets, respectively. From these figures, we can see that model architecture has observable effect on prediction performance. In addition, when comparing the performance of BiLSTM and UniLSTM by considering the sum of MAE of SBP and DBP, UniLSTM consistently showed inferior results across all training settings in both datasets, particularly when trained with min-max normalization per signal. This suggests that utilizing bidirectional LSTM layers to capture forward and backward information flow of PPG-signals is more effective for BP prediction. Moreover, for certain training settings, the performance of UniLSTM did not differ from the baseline mean predictor, indicating the incapability of unidirectional LSTM layers in this task. Based on this observation, we simply excluded UniLSTM from further experiments.

Figures 8 and 9 show the the performance of the models averaged by HR feature for SBP and DBP prediction on the MIMIC-III subset from PulseDB. With referring to these figures, we can see that the inclusion of HR as an additional feature for BP estimation did not yield an observable improvement in model performance. This same phenomenon is also observed on the MIMIC-III subset from Kaggle.

Figures 10 and 11 show the performance of the models averaged by task-based learning for SBP and DBP prediction on the MIMIC-III subset from PulseDB. We can see that single-task learning does not lead to an observable improvement in model performance. This same phenomenon is observed on the MIMIC-III subset from Kaggle as well. Consequently, to conserve computational resources and reduce training time, all subsequent experiments were conducted using multi-task learning.

In the MIMIC-III subset from Kaggle, BiLSTM trained with min-max normalization per signal and without HR as a feature in a multi-task learning manner achieved the lowest MAE with 11.121 mmHg and 5.523 mmHg for SBP and

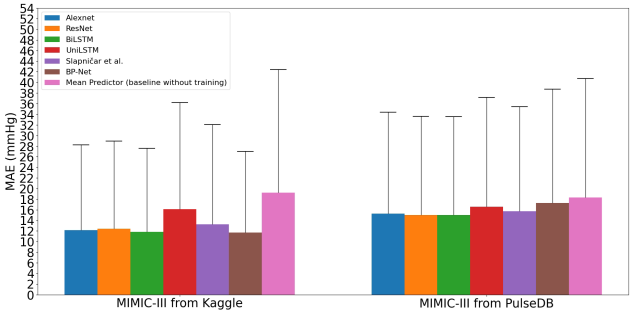

Figure 6. MAEs in SBP prediction using PPG signals evaluated across different models in two PPG datasets (averaging all combinations of normalization methods, single-task / multi-task, and with / without HR). Mean Predictor is the baseline reference.

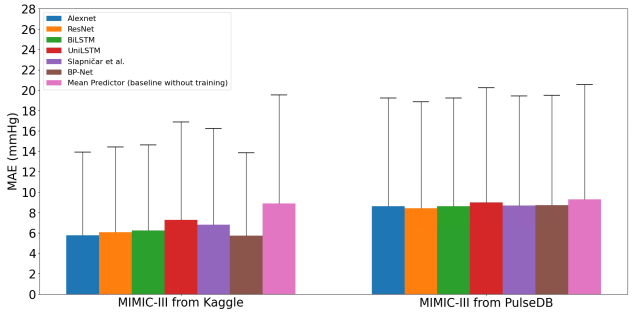

Figure 7. MAEs in DBP prediction using PPG signals evaluated across different models in two PPG datasets (averaging all combinations of normalization methods, single-task / multi-task, and with / without HR). Mean Predictor is the baseline reference.

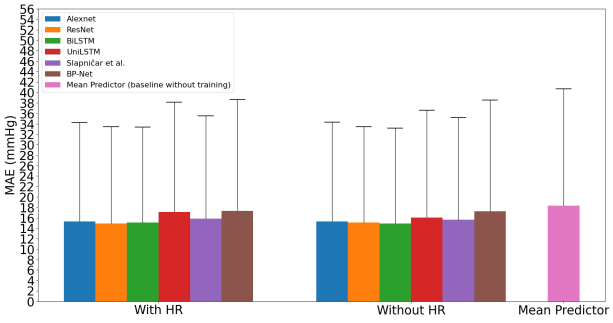

Figure 8. Illustrating the lack of influence of the presence or absence of HR during training on MAE in SBP prediction using PPG signals in MIMIC-III subset from PulseDB. Mean predictor is the baseline reference.

DBP, respectively. In the MIMIC-III subset from PulseDB, the model proposed by Slapničar et al. trained with min-max normalization per signal and without HR as a feature in a single-task learning manner attained the lowest MAE with 14.936 mmHg and 8.179 mmHg for SBP and DBP, respectively. The performance difference between these two PPG

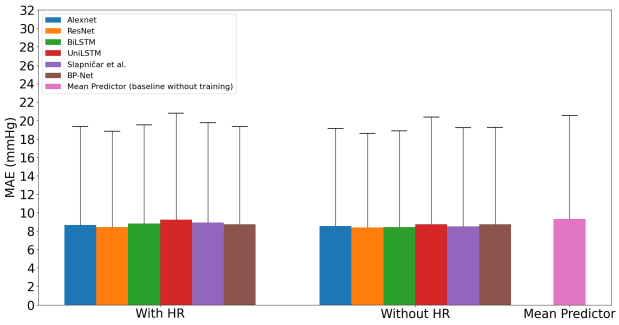

Figure 9. Illustrating the lack of influence of the presence or absence of HR during training on MAE in DBP prediction using PPG signals in MIMIC-III subset from PulseDB. Mean predictor is the baseline reference.

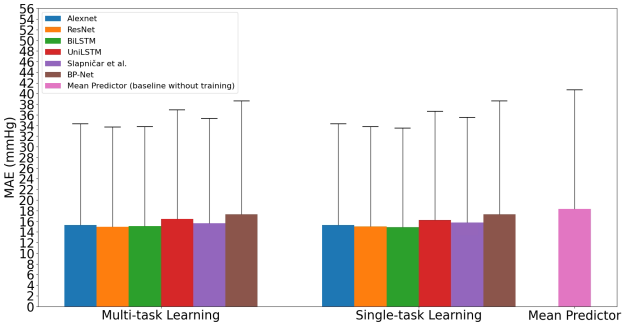

Figure 10. Illustrating the lack of influence of multi-task or single-task learning on MAE in SBP prediction using PPG signals in MIMIC-III subset from PulseDB. Mean predictor is the baseline reference.

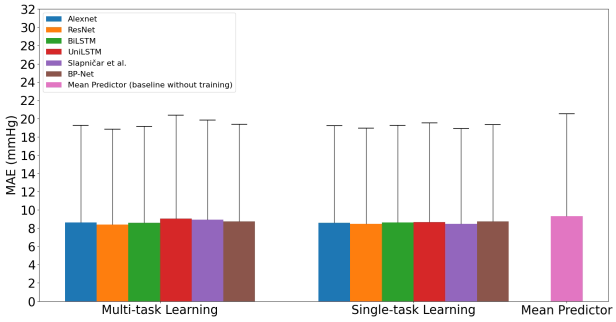

Figure 11. Illustrating the lack of influence of multi-task or single-task learning on MAE in DBP prediction using PPG signals in MIMIC-III subset from PulseDB. Mean predictor is the baseline reference.

datasets might be due to data leakage, as one patient could have multiple records in the MIMIC-III subset from Kaggle, with no information available to distinguish between them. The performance of the models with respect to each training setting can be found in the supplementary material.

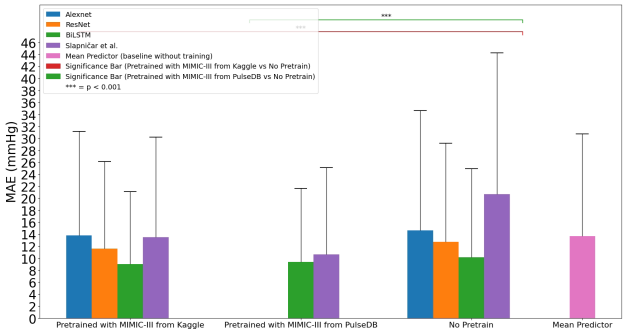

Figure 12. Benefits of pretraining in reducing MAE in SBP prediction of selected models with specific training setting.

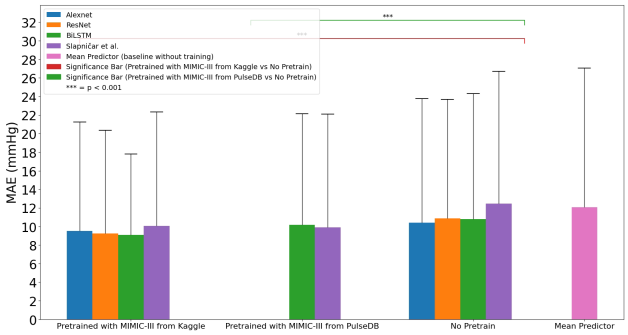

Figure 13. Benefits of pretraining in reducing MAE in DBP prediction of selected models with specific training setting.

4.2. Blood Pressure Estimation by Transfer Learning with rPPG Data

Figures 12 and 13 show the performance of selected models with specific training setting for SBP and DBP prediction on the rPPG-LUH. From these figures, we can observe that models that are either pretrained on MIMIC-III from Kaggle or MIMIC-II from PulseDB have a better performance than those without pretrain. Paired t-tests (Pretrained with MIMIC-III from Kaggle vs No Pretrain, and Pretrain with MIMIC-III from PulseDB vs No Pretrain) are also performed for all training settings of each model and the results show that the transfer learning approach consistently leads to significant difference in model performance (T-value $>$ T_c or T-value $<$ -T_c and p-value $<$ 0.05). Meanwhile, for SBP prediction, Alexnet performed worse than the baseline mean predictor. This may be due to the limited sample size of the rPPG-LUH and the model architecture in handling noisy rPPG signals.

Further analysis reveals a consistent improvement in predicting SBP by ResNet and BiLSTM when using HR values estimated from relatively noisy rPPG-signals. However, this improvement is not observed during the pretrain stage. This may be due to the size of the dataset and the quality of the signals. As in the pretrain stage, the two

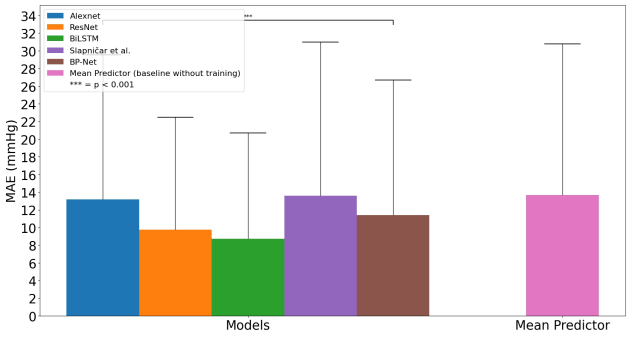

Figure 14. Illustrating MAEs in SBP prediction by different pretrained models with the training setting: pretrained with MIMIC-III from Kaggle, normalization per dataset, MAE loss function, and with HR feature. Mean predictor is the baseline reference.

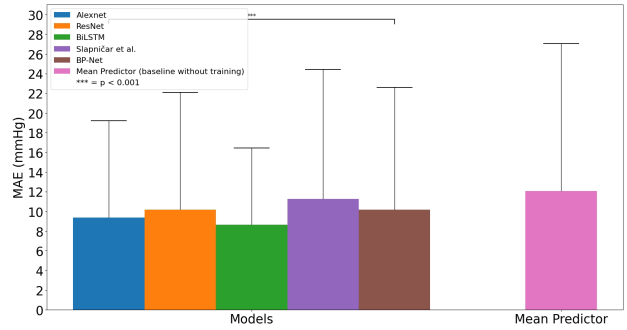

Figure 15. Illustrating MAEs in DBP prediction by different pretrained models with the training setting: pretrained with MIMIC-III from Kaggle, normalization per dataset, MAE loss function, and with HR feature. Mean predictor is the baseline reference.

PPG datasets were much larger than the rPPG dataset and they provided more diverse samples. Also, those PPG-signals were collected with specialized medical devices, which contain fewer noises than rPPG-signals. This allows models to learn more robust and generalisable features for BP prediction. Therefore, HR may not add much new information beyond what the models have already learned from the PPG-signals. In contrast, as the size of the rPPG dataset is much smaller and the signals are noisier due to illumination environments, motion artifacts or camera quality, using HR as an additional information may help models disentangle useful information from noises, leading to better BP prediction. Therefore, experiments with larger and cleaner rPPG datasets are necessary to analyse the importance of HR for BP estimation.

To statistically analyse the factors affecting BP prediction performance, we conducted analysis of variance (ANOVA) tests based on model architectures, and paired t-tests based on pretrain datasets, normalization methods, loss functions and the introduction of HR. For the ANOVA

Method	MAE (mmHg) SBP	MAE (mmHg) DBP	Evaluation Approach
[66]	13.6	10.3	leave-two-out cross validation
[38]	6.9	4.43	20% data with potential subject overlapping
This Paper	8.721	8.653	4-Fold without subject overlapping

Table 1. Performance comparison of different methods with different evaluation approaches on the same rPPG dataset (rPPG-LUH).

tests, the F-values and p-values based on model architectures were $> F_c$ and < 0.05, respectively, for both SBP and DBP in all training settings, indicating that using different deep learning models for BP prediction lead to significant difference in model performance. Figures 14 and 15 show the performance of the models with specific training setting for SBP and DBP prediction on the rPPG-LUH. For the paired t-tests, the T-values and p-values based on pretrain datasets, normalization methods, loss functions and the introduction of HR were $> T_c$ or $< -T_c$ and < 0.05 only for certain training settings, preventing us from concluding any specific factor that consistently leads to significant difference in model performance.

BiLSTM that pretrained on the MIMIC-III subset from Kaggle, and then fine-tuned on rPPG-signals and HR, with min-max normalization per dataset and MAE loss function achieved the lowest MAE of 8.721 mmHg and 8.653 mmHg for SBP and DBP, respectively. By applying transfer learning, fine-tuned BiLSTM improved the MAE for SBP by 27.65% and 36.23% compared to BiLSTM without fine-tuning and mean predictor, respectively. For DBP, fine-tuned BiLSTM improved the MAE by 11.68% and 28.27% compared to BiLSTM without fine-tuning and mean predictor, respectively. Although both SBP and DBP are critical indicators for cardiovascular risk, several studies have shown that SBP is more sensitive to cardiovascular diseases, especially in older adults [4, 37]. This makes using HR as a feature for BP estimation more favourable as it improves the accuracy of BiLSTM in predicting SBP in all training settings, which can be observed in figure 16. To further illustrate its performance, we compared it with international protocols for BP measurement, including British Hypertension Society (BHS) [79] and AAMI standards. The model attained Grade C for both SBP and DBP according to the BHS standards. Meanwhile, it did not meet the AAMI standards for SBP and this presents an opportunity for further refinement. Table 1 shows the comparison of the performance with other studies evaluated on the same rPPG dataset (rPPG-LUH). The performance of the models with respect to each training setting and the results of the statistical tests can be found in the supplementary material.

5. Conclusion and Future Works

In this study, we benchmarked various deep learning models pretrained on diverse public PPG datasets, subsequently fine-tuning them utilizing a public rPPG dataset. Initially, PPG-signals and rPPG-signals underwent preprocessing and segmentation to enhance signal quality before being utilized for cross-validation. We also evaluated different loss functions and normalization approaches to optimize the training settings for the deep learning models. Our results demonstrate that fine-tuning pretrained PPG models with limited rPPG data and HR led to substantial enhancements in model performance, as evidenced by the attainment of MAE, with 8.721 mmHg and 8.653 mmHg for SBP and DBP, respectively, in a clinical dataset.

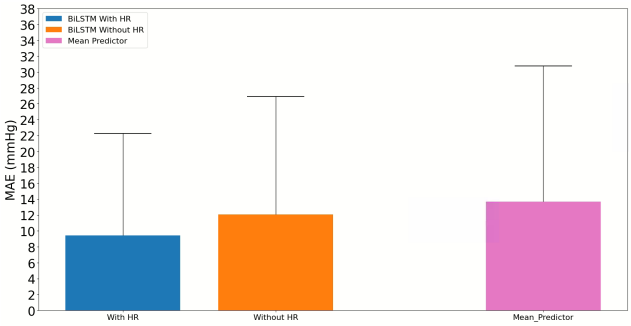

Figure 16. MAE in SBP prediction (averaged by HR feature) by pretrained BiLSTM is significantly reduced by the presence of the HR feature. Mean Predictor is the baseline reference.

There are three directions future research should take. Firstly, to tackle the inherent unevenness in the distribution of SBP and DBP within rPPG datasets, we intend to explore diverse resampling techniques and data augmentation methods, aiming to improve the model's generalisation capabilities. Combining multiple rPPG datasets may also address this challenge. However, unlike recording PPG data with standard medical devices, rPPG data are extracted based on specific setups (e.g., cameras, illumination environments and rPPG-signal extraction algorithms) in different datasets. These setups can vary significantly, and combining them for model training may result in poor performance. Therefore, we would greatly appreciate the establishment of a standard setup agreed upon by domain experts so that rPPG datasets collected under certain systems can be utilized together. Secondly, the incorporation of cutting-edge deep learning architectures such as transformer for BP estimation constitutes a pivotal avenue for further investigation. Thirdly, in order to enhance the performance of vital sign monitoring, there is a growing interest in exploring various deep learning methodologies for the extraction of rPPG-signals. These alternative approaches have the potential to generate more realistic rPPG-signals that resembling PPG-signals. Integrating such methods may be able to further improve the accuracy and effectiveness of BP prediction models.

References

[1] Yusuke Akamatsu, Yoshifumi Onishi, and Hitoshi Imaoka. Blood oxygen saturation estimation from facial video via dc and ac components of spatio-temporal map. In *ICASSP 2023-2023 IEEE International Conference on Acoustics, Speech and Signal Processing (ICASSP)*, pages 1–5. IEEE, 2023. 2

[2] Noor Faris Ali and Mohamed Atef. An efficient hybrid lstm-ann joint classification-regression model for ppg based blood pressure monitoring. *Biomedical Signal Processing and Control*, 84:104782, 2023. 1

[3] Malak Abdullah Almarshad, Md Saiful Islam, Saad Al-Ahmadi, and Ahmed S BaHammam. Diagnostic features and potential applications of ppg signal in healthcare: A systematic review. In *Healthcare*, volume 10, page 547. MDPI, 2022. 1

[4] Sripal Bangalore, Franz H Messerli, Stanley S Franklin, Giuseppe Mancia, Annette Champion, and Carl J Pepine. Pulse pressure and risk of cardiovascular outcomes in patients with hypertension and coronary artery disease: an international verapamil sr-trandolapril study (invest) analysis. *European heart journal*, 30(11):1395–1401, 2009. 8

[5] Gareth Beevers, Gregory YH Lip, and Eoin O'Brien. Blood pressure measurement: Part i—sphygmomanometry: Factors common to all techniques. *Bmj*, 322(7292):981–985, 2001. 1

[6] Dwaipayan Biswas, Neide Simões-Capela, Chris Van Hoof, and Nick Van Helleputte. Heart rate estimation from wrist-worn photoplethysmography: A review. *IEEE Sensors Journal*, 19(16):6560–6570, 2019. 1

[7] Giuseppe Boccignone, Donatello Conte, Vittorio Cuculo, Alessandro d'Amelio, Giuliano Grossi, and Raffaella Lanzarotti. An open framework for remote-ppg methods and their assessment. *IEEE Access*, 8:216083–216103, 2020. 4

[8] Denisse Castaneda, Aibhlin Esparza, Mohammad Ghamari, Cinna Soltanpur, and Homer Nazeran. A review on wearable photoplethysmography sensors and their potential future applications in health care. *International journal of biosensors & bioelectronics*, 4(4):195, 2018. 1

[9] Peter H Charlton, Drew A Birrenkott, Timothy Bonnici, Marco AF Pimentel, Alistair EW Johnson, Jordi Alastruey, Lionel Tarassenko, Peter J Watkinson, Richard Beale, and David A Clifton. Breathing rate estimation from the electrocardiogram and photoplethysmogram: A review. *IEEE reviews in biomedical engineering*, 11:2–20, 2017. 1

[10] Wei Chen, Dezhao Zhai, Hang Wu, Zhu Luo, Fulong Liu, Yijing Fu, Yan Chen, and Xiaotao Zhang. Non-contact blood pressure detection based on weighted ensemble learning model. *Signal, Image and Video Processing*, 18(1):553–560, 2024. 2

[11] Xi Chen, Yan Duan, Rein Houthooft, John Schulman, Ilya Sutskever, and Pieter Abbeel. Infogan: Interpretable representation learning by information maximizing generative adversarial nets. *Advances in neural information processing systems*, 29, 2016. 2

[12] Yuheng Chen, Jialiang Zhuang, Bin Li, Yun Zhang, and Xiujuan Zheng. Remote blood pressure estimation via the spatiotemporal mapping of facial videos. *Sensors*, 23(6):2963, 2023. 2

[13] Chun-Hong Cheng, Kwan-Long Wong, Jing-Wei Chin, Tsz-Tai Chan, and Richard HY So. Deep learning methods for remote heart rate measurement: A review and future research agenda. *Sensors*, 21(18):6296, 2021. 1

[14] Chun-Hong Cheng, Zhikun Yuen, Shutao Chen, Kwan-Long Wong, Jing-Wei Chin, Tsz-Tai Chan, and Richard HY So. Contactless blood oxygen saturation estimation from facial videos using deep learning. *Bioengineering*, 11(3):251, 2024. 2

[15] Kyunghyun Cho, Bart Van Merriënboer, Caglar Gulcehre, Dzmitry Bahdanau, Fethi Bougares, Holger Schwenk, and Yoshua Bengio. Learning phrase representations using rnn encoder-decoder for statistical machine translation. *arXiv preprint arXiv:1406.1078*, 2014. 2

[16] Yan Chu, Kaichen Tang, Yu-Chun Hsu, Tongtong Huang, Dulin Wang, Wentao Li, Sean I Savitz, Xiaoqian Jiang, and Shayan Shams. Non-invasive arterial blood pressure measurement and spo2 estimation using ppg signal: A deep learning framework. *BMC Medical Informatics and Decision Making*, 23(1):131, 2023. 1

[17] Theodore Curran, Daniel McDuff, Xin Liu, Girish Narayanswamy, Chengqian Ma, Shwetak Patel, and Eugene Yang. Camera-based remote photoplethysmography for blood pressure measurement: current evidence, clinical perspectives, and future applications. *Connected Health Telemedicine*, 2(2), 2023. 1

[18] Gerard De Haan and Vincent Jeanne. Robust pulse rate from chrominance-based rppg. *IEEE Transactions on Biomedical Engineering*, 60(10):2878–2886, 2013. 1

[19] Javier de Pedro-Carracedo, Ana María Ugena, and Ana Pilar Gonzalez-Marcos. Dynamical analysis of biological signals with the 0–1 test: a case study of the photoplethysmographic (ppg) signal. *Applied Sciences*, 11(14):6508, 2021. 4

[20] Hoda El Boussaki, Rachid Latif, and Amine Saddik. A review on video-based heart rate, respiratory rate and blood pressure estimation. In *International Conference of Machine Learning and Computer Science Applications*, pages 129–140. Springer, 2022. 1

[21] Chadi El Hajj and Panayiotis A Kyriacou. Cuffless and continuous blood pressure estimation from ppg signals using recurrent neural networks. In *2020 42nd annual international conference of the IEEE engineering in medicine & biology society (EMBC)*, pages 4269–4272. IEEE, 2020. 1, 2

[22] Chadi El-Hajj and Panayiotis A Kyriacou. Cuffless blood pressure estimation from ppg signals and its derivatives using deep learning models. *Biomedical Signal Processing and Control*, 70:102984, 2021. 1, 2

[23] Jamal Esmaelpoor, Mohammad Hassan Moradi, and Abdolrahim Kadkhodamohammadi. A multistage deep neural network model for blood pressure estimation using photoplethysmogram signals. *Computers in Biology and Medicine*, 120:103719, 2020. 1, 2

[24] Flávio D Fuchs and Paul K Whelton. High blood pressure and cardiovascular disease. *Hypertension*, 75(2):285–292, 2020. 1

[25] Munenori Fukunishi, Kouki Kurita, Shoji Yamamoto, and Norimichi Tsumura. Non-contact video-based estimation of heart rate variability spectrogram from hemoglobin composition. *Artificial Life and Robotics*, 22:457–463, 2017. 2

[26] Ankit Gupta, Antonio G Ravelo-García, and Fernando Morgado-Dias. Recent advancements in deep learning-based remote photoplethysmography methods. *Data Fusion Techniques and Applications for Smart Healthcare*, pages 127–155, 2024. 1

[27] Shresth Gupta, Anurag Singh, Abhishek Sharma, and Rajesh Kumar Tripathy. Higher order derivative-based integrated model for cuff-less blood pressure estimation and stratification using ppg signals. *IEEE sensors journal*, 22(22):22030–22039, 2022. 1

[28] Xuesong Han, Xuezhi Yang, Shuai Fang, Yawei Chen, Qin Chen, Longwei Li, and RenCheng Song. Preserving shape details of pulse signals for video-based blood pressure estimation. *Biomedical Optics Express*, 15(4):2433–2450, 2024. 2

[29] Xuesong Han, Xuezhi Yang, Shuai Fang, Rencheng Song, Longwei Li, and Jie Zhang. Non-contact blood pressure estimation using bp-related cardiovascular knowledge: an uncalibrated method based on consumer-level camera. *IEEE Transactions on Instrumentation and Measurement*, 2023. 2

[30] Kaiming He, Xiangyu Zhang, Shaoqing Ren, and Jian Sun. Deep residual learning for image recognition. In *Proceedings of the IEEE conference on computer vision and pattern recognition*, pages 770–778, 2016. 2, 3

[31] Abdulkader Helwan, Danielle Azar, and Mohamad Khaleel Sallam Ma'aitah. Conventional and deep learning methods in heart rate estimation from rgb face videos. *Physiological Measurement*, 45(2):02TR01, 2024. 1

[32] Sepp Hochreiter and Jürgen Schmidhuber. Long short-term memory. *Neural computation*, 9(8):1735–1780, 1997. 2

[33] Min Hu, Xia Wu, Xiaohua Wang, Yan Xing, Ning An, and Piao Shi. Contactless blood oxygen estimation from face videos: A multi-model fusion method based on deep learning. *Biomedical Signal Processing and Control*, 81:104487, 2023. 1

[34] Kaito Iuchi, Ryogo Miyazaki, George C Cardoso, Keiko Ogawa-Ochiai, and Norimichi Tsumura. Remote estimation of continuous blood pressure by a convolutional neural network trained on spatial patterns of facial pulse waves. In *Proceedings of the IEEE/CVF Conference on Computer Vision and Pattern Recognition*, pages 2139–2145, 2022. 2

[35] Kjel A Johnson, Deborah J Partsch, Patrick Gleason, and Kelly Makay. Comparison of two home blood pressure monitors with a mercury sphygmomanometer in an ambulatory population. *Pharmacotherapy: The Journal of Human Pharmacology and Drug Therapy*, 19(3):333–339, 1999. 1

[36] Mohamad Kachuee, Mohammad Mahdi Kiani, Hoda Mohammadzade, and Mahdi Shabany. Cuff-less high-accuracy calibration-free blood pressure estimation using pulse transit time. In *2015 IEEE international symposium on circuits and systems (ISCAS)*, pages 1006–1009. IEEE, 2015. 3, 4

[37] Ashish K Khanna, Takahiro Kinoshita, Annamalai Natarajan, Emma Schwager, Dustin D Linn, Junzi Dong, Erina Ghosh, Francesco Vicario, and Kamal Maheshwari. Association of systolic, diastolic, mean, and pulse pressure with morbidity and mortality in septic icu patients: a nationwide observational study. *Annals of Intensive Care*, 13(1):9, 2023. 8

[38] Seunghyun Kim, Hyeji Lim, Junho Baek, and Eui Chul Lee. Rgb camera-based blood pressure measurement using u-net basic generative model. *Electronics*, 12(18):3771, 2023. 3, 8

[39] Diederik P Kingma and Jimmy Ba. Adam: A method for stochastic optimization. *arXiv preprint arXiv:1412.6980*, 2014. 4

[40] Walter M Kirkendall, ALAN C BURTON, FREDERICK H EPSTEIN, and EDWARD D FREIS. Recommendations for human blood pressure determination by sphygmomanometers. *Circulation*, 36(6):980–988, 1967. 1

[41] Alex Krizhevsky, Ilya Sutskever, and Geoffrey E Hinton. Imagenet classification with deep convolutional neural networks. *Advances in neural information processing systems*, 25, 2012. 3

[42] Paola A Lanfranchi and Virend K Somers. Arterial baroreflex function and cardiovascular variability: interactions and implications. *American Journal of Physiology-Regulatory, Integrative and Comparative Physiology*, 283(4):R815–R826, 2002. 2

[43] Hyung-Chul Lee, Yoonsang Park, Soo Bin Yoon, Seong Mi Yang, Dongnyeok Park, and Chul-Woo Jung. Vitaldb, a high-fidelity multi-parameter vital signs database in surgical patients. *Scientific Data*, 9(1):279, 2022. 3

[44] Ru Jing Lee, Saaveethya Sivakumar, and King Hann Lim. Review on remote heart rate measurements using photoplethysmography. *Multimedia Tools and Applications*, pages 1–30, 2023. 1

[45] Magdalena Lewandowska, Jacek Rumiński, Tomasz Kocejko, and Jedrzej Nowak. Measuring pulse rate with a webcam—a non-contact method for evaluating cardiac activity. In *2011 Federated Conference on Computer Science and Information Systems (FedCSIS)*, pages 405–410. IEEE, 2011. 1

[46] Hao Liang, Wei He, and Zheng Xu. A deep learning method for continuous noninvasive blood pressure monitoring using photoplethysmography. *Physiological Measurement*, 44(5):055004, 2023. 1, 2

[47] Haipeng Liu, John Allen, Dingchang Zheng, and Fei Chen. Recent development of respiratory rate measurement technologies. *Physiological measurement*, 40(7):07TR01, 2019. 1

[48] Jiankun Liu, Hao-Min Cheng, Chen-Huan Chen, Shih-Hsien Sung, Mohsen Moslehpour, Jin-Oh Hahn, and Ramakrishna Mukkamala. Patient-specific oscillometric blood pressure measurement. *IEEE Transactions on Biomedical Engineering*, 63(6):1220–1228, 2015. 1

[49] Xin Liu, Yuting Zhang, Zitong Yu, Hao Lu, Huanjing Yue, and Jingyu Yang. rppg-mae: Self-supervised pretraining with masked autoencoders for remote physiological measurements. *IEEE Transactions on Multimedia*, 2024. 2

[50] Ye Lu, Chaoqun Wang, and Max Q-H Meng. Video-based contactless blood pressure estimation: A review. In *2020*

IEEE International Conference on Real-time Computing and Robotics (RCAR), pages 62–67. IEEE, 2020. 1

[51] Ping-Kwan Man, Kit-Leong Cheung, Nawapon Sangsiri, Wilfred Jin Shek, Kwan-Long Wong, Jing-Wei Chin, Tsz-Tai Chan, and Richard Hau-Yue So. Blood pressure measurement: From cuff-based to contactless monitoring. In *Healthcare*, volume 10, page 2113. MDPI, 2022. 1

[52] Joshua Mathew, Xin Tian, Chau-Wai Wong, Simon Ho, Donald K Milton, and Min Wu. Remote blood oxygen estimation from videos using neural networks. *IEEE journal of biomedical and health informatics*, 2023. 1

[53] David J Meredith, D Clifton, P Charlton, J Brooks, CW Pugh, and L Tarassenko. Photoplethysmographic derivation of respiratory rate: a review of relevant physiology. *Journal of medical engineering & technology*, 36(1):1–7, 2012. 1

[54] Xuesong Niu, Hu Han, Shiguang Shan, and Xilin Chen. Synrhythm: Learning a deep heart rate estimator from general to specific. In *2018 24th international conference on pattern recognition (ICPR)*, pages 3580–3585. IEEE, 2018. 2

[55] Xuesong Niu, Shiguang Shan, Hu Han, and Xilin Chen. Rhythmnet: End-to-end heart rate estimation from face via spatial-temporal representation. *IEEE Transactions on Image Processing*, 29:2409–2423, 2019. 2

[56] Xuesong Niu, Zitong Yu, Hu Han, Xiaobai Li, Shiguang Shan, and Guoying Zhao. Video-based remote physiological measurement via cross-verified feature disentangling. In *Computer Vision–ECCV 2020: 16th European Conference, Glasgow, UK, August 23–28, 2020, Proceedings, Part II 16*, pages 295–310. Springer, 2020. 2

[57] Xuesong Niu, Xingyuan Zhao, Hu Han, Abhijit Das, Antitza Dantcheva, Shiguang Shan, and Xilin Chen. Robust remote heart rate estimation from face utilizing spatial-temporal attention. In *2019 14th IEEE international conference on automatic face & gesture recognition (FG 2019)*, pages 1–8. IEEE, 2019. 2

[58] Pankaj, Ashish Kumar, Rama Komaragiri, and Manjeet Kumar. A review on computation methods used in photoplethysmography signal analysis for heart rate estimation. *Archives of Computational Methods in Engineering*, 29(2):921–940, 2022. 1

[59] Junyung Park, Hyeon Seok Seok, Sang-Su Kim, and Hangsik Shin. Photoplethysmogram analysis and applications: An integrative review. *Frontiers in Physiology*, 12:808451, 2022. 1

[60] Jiahe Peng, Weihua Su, Haiyong Chen, Jingsheng Sun, and Zandong Tian. Cl-spo2net: Contrastive learning spatiotemporal attention network for non-contact video-based spo2 estimation. *Bioengineering*, 11(2):113, 2024. 1

[61] Vijitha Periyasamy, Manojit Pramanik, and Prasanta Kumar Ghosh. Review on heart-rate estimation from photoplethysmography and accelerometer signals during physical exercise. *Journal of the Indian Institute of Science*, 97:313–324, 2017. 1

[62] Christian S Pilz, Sebastian Zaunseder, Jarek Krajewski, and Vladimir Blazek. Local group invariance for heart rate estimation from face videos in the wild. In *Proceedings of the IEEE conference on computer vision and pattern recognition workshops*, pages 1254–1262, 2018. 1

[63] Ming-Zher Poh, Daniel J McDuff, and Rosalind W Picard. Non-contact, automated cardiac pulse measurements using video imaging and blind source separation. *Optics express*, 18(10):10762–10774, 2010. 1

[64] Olaf Ronneberger, Philipp Fischer, and Thomas Brox. U-net: Convolutional networks for biomedical image segmentation. In *Medical image computing and computer-assisted intervention–MICCAI 2015: 18th international conference, Munich, Germany, October 5-9, 2015, proceedings, part III 18*, pages 234–241. Springer, 2015. 2

[65] Pantelis A Sarafidis, Panagiotis I Georgianos, Antonios Karpetas, Athanasios Bikos, Linda Korelidou, Maria Tersi, Dimitrios Divanis, Georgios Tzanis, Konstantinos Mavromatidis, Vassilios Liakopoulos, et al. Evaluation of a novel brachial cuff-based oscillometric method for estimating central systolic pressure in hemodialysis patients. *American Journal of Nephrology*, 40(3):242–250, 2014. 1

[66] Fabian Schrumpf, Patrick Frenzel, Christoph Aust, Georg Osterhoff, and Mirco Fuchs. Assessment of non-invasive blood pressure prediction from ppg and rppg signals using deep learning. *Sensors*, 21(18):6022, 2021. 2, 3, 4, 8

[67] Toshihiro Shoji, Atsushi Nakagomi, Sho Okada, Yuji Ohno, and Yoshio Kobayashi. Invasive validation of a novel brachial cuff-based oscillometric device (sphygmocor xcel) for measuring central blood pressure. *Journal of hypertension*, 35(1):69–75, 2017. 1

[68] Gasper Slapničar, Mitja Luštrek, and Matej Marinko. Continuous blood pressure estimation from ppg signal. *Informatica*, 42(1), 2018. 1, 2

[69] Gašper Slapničar, Nejc Mlakar, and Mitja Luštrek. Blood pressure estimation from photoplethysmogram using a spectro-temporal deep neural network. *Sensors*, 19(15):3420, 2019. 1, 3

[70] Xiantao Sun, Tao Wen, Weihai Chen, and Bin Huang. Ccspo 2 net: Camera-based contactless oxygen saturation measurement foundation model in clinical settings. *IEEE Transactions on Instrumentation and Measurement*, 2024. 1

[71] Ali Tazarv and Marco Levorato. A deep learning approach to predict blood pressure from ppg signals. In *2021 43rd Annual international conference of the IEEE engineering in medicine & biology society (EMBC)*, pages 5658–5662. IEEE, 2021. 1

[72] Ulrich Tholl, Klaus Forstner, and Manfred Anlauf. Measuring blood pressure: Pitfalls and recommendations. *Nephrology Dialysis Transplantation*, 19(4):766–770, 2004. 1

[73] K Rishi Vardhan, S Vedanth, G Poojah, K Abhishek, M Nitish Kumar, and Vineeth Vijayaraghavan. Bp-net: Efficient deep learning for continuous arterial blood pressure estimation using photoplethysmogram. In *2021 20th IEEE International Conference on Machine Learning and Applications (ICMLA)*, pages 1495–1500. IEEE, 2021. 3

[74] Ramachandran S Vasan, Martin G Larson, Eric P Leip, Jane C Evans, Christopher J O'Donnell, William B Kannel, and Daniel Levy. Impact of high-normal blood pressure on the risk of cardiovascular disease. *New England journal of medicine*, 345(18):1291–1297, 2001. 1

[75] Di Wang, Yutong Ye, Bowen Zhang, Jinlu Sun, and Cheng Zhang. Imsf-net: An improved multi-scale information

fusion network for ppg-based blood pressure estimation. *Biomedical Signal Processing and Control*, 90:105791, 2024. 1, 2

[76] Wenjin Wang, Albertus C Den Brinker, Sander Stuijk, and Gerard De Haan. Algorithmic principles of remote ppg. *IEEE Transactions on Biomedical Engineering*, 64(7):1479–1491, 2016. 1, 2

[77] Weinan Wang, Pedram Mohseni, Kevin L Kilgore, and Laleh Najafizadeh. Pulsedb: A large, cleaned dataset based on mimic-iii and vitaldb for benchmarking cuff-less blood pressure estimation methods. *Frontiers in Digital Health*, 4:1090854, 2023. 3, 4

[78] Thomas Weber, Siegfried Wassertheurer, Martin Rammer, Edwin Maurer, Bernhard Hametner, Christopher C Mayer, Johannes Kropf, and Bernd Eber. Validation of a brachial cuff-based method for estimating central systolic blood pressure. *Hypertension*, 58(5):825–832, 2011. 1

[79] Bryan Williams, NR Poulter, MJ Brown, M Davis, GT McInnes, JF Potter, PS Sever, and S McG Thom. Guidelines for management of hypertension: report of the fourth working party of the british hypertension society, 2004—bhs iv. *Journal of human hypertension*, 18(3):139–185, 2004. 8

[80] Bing-Fei Wu, Li-Wen Chiu, Yi-Chiao Wu, Chun-Chih Lai, and Pao-Hsien Chu. Contactless blood pressure measurement via remote photoplethysmography with synthetic data generation using generative adversarial network. In *Proceedings of the IEEE/CVF Conference on Computer Vision and Pattern Recognition*, pages 2130–2138, 2022. 2

[81] Bing-Fei Wu, Bing-Jhang Wu, Bing-Ruei Tsai, and Chi-Po Hsu. A facial-image-based blood pressure measurement system without calibration. *IEEE Transactions on Instrumentation and Measurement*, 71:1–13, 2022. 2

[82] Hanguang Xiao, Tianqi Liu, Yisha Sun, Yulin Li, Shiyi Zhao, and Alberto Avolio. Remote photoplethysmography for heart rate measurement: A review. *Biomedical Signal Processing and Control*, 88:105608, 2024. 1

[83] Yue Zhang and Zhimeng Feng. A svm method for continuous blood pressure estimation from a ppg signal. In *Proceedings of the 9th international conference on machine learning and computing*, pages 128–132, 2017. 1

[84] Zheng Zhang, Jeff M Girard, Yue Wu, Xing Zhang, Peng Liu, Umur Ciftci, Shaun Canavan, Michael Reale, Andy Horowitz, Huiyuan Yang, et al. Multimodal spontaneous emotion corpus for human behavior analysis. In *Proceedings of the IEEE conference on computer vision and pattern recognition*, pages 3438–3446, 2016. 2